

# PCCP

Accepted Manuscript



This is an *Accepted Manuscript*, which has been through the Royal Society of Chemistry peer review process and has been accepted for publication.

*Accepted Manuscripts* are published online shortly after acceptance, before technical editing, formatting and proof reading. Using this free service, authors can make their results available to the community, in citable form, before we publish the edited article. We will replace this *Accepted Manuscript* with the edited and formatted *Advance Article* as soon as it is available.

You can find more information about *Accepted Manuscripts* in the [Information for Authors](#).

Please note that technical editing may introduce minor changes to the text and/or graphics, which may alter content. The journal's standard [Terms & Conditions](#) and the [Ethical guidelines](#) still apply. In no event shall the Royal Society of Chemistry be held responsible for any errors or omissions in this *Accepted Manuscript* or any consequences arising from the use of any information it contains.

# Photon Management Properties of Rare-Earth (Nd, Yb, Sm)-Doped CeO<sub>2</sub> Films Prepared by Pulsed Laser Deposition

Matteo Balestrieri<sup>1,\*</sup>, Silviu Colis<sup>1,\*</sup>, Mathieu Gallart<sup>1</sup>, Guy Schmerber<sup>1</sup>, Paul Bazylewski<sup>2</sup>, Gap Soo Chang<sup>2</sup>, Marc Ziegler<sup>1</sup>, Pierre Gilliot<sup>1</sup>, Abdelilah Slaoui<sup>3</sup> and Aziz Dinia<sup>1</sup>

<sup>1</sup> *Institut de Physique et Chimie des Matériaux de Strasbourg, Université de Strasbourg, CNRS UMR 7504, 23 rue du Loess, B.P. 43, F-67034 Strasbourg Cedex 2, France*

<sup>2</sup> *Department of Physics and Engineering Physics, University of Saskatchewan, 116 Science Place, Saskatoon, SK S7N 5E2, Canada*

<sup>3</sup> *Laboratoire ICube, Université de Strasbourg, CNRS UMR 7357, 23 rue du Loess, B.P. 20, F-67037 Strasbourg Cedex 2, France*

## Corresponding authors

\*Matteo Balestrieri : [m\\_balestrieri@libero.it](mailto:m_balestrieri@libero.it)

\*Silviu Colis: [colis@ipcms.unistra.fr](mailto:colis@ipcms.unistra.fr), +33 3 88 10 71 29

**Abstract**

CeO<sub>2</sub> is a promising material for applications in optoelectronics and photovoltaics due to its large band gap and to values of the refractive index and of the lattice parameter that are suitable for silicon-based devices. In this work, we show that trivalent Sm, Nd and Yb ions can be successfully inserted and optically activated in CeO<sub>2</sub> films grown at a relatively low deposition temperature (400 °C), which is compatible with inorganic photovoltaics. CeO<sub>2</sub> thin films can therefore be efficiently functionalized with photon-management properties by doping with trivalent rare earth (RE) ions. The structural and optical analyses provide details of the electronic level structure of the films and of the energy transfer mechanisms. In particular, we give evidence of the existence of an absorption band centered at 350 nm from which energy transfer occurs to the rare-earth ions. The transfer mechanisms can be completely explained only by considering the spontaneous migration of Ce<sup>3+</sup> ions in CeO<sub>2</sub> at a short distance from the RE<sup>3+</sup> ions. The strong absorption cross section of f-d transitions in Ce<sup>3+</sup> ions efficiently intercepts the UV photons of the solar spectrum and therefore strongly increases the potential of these layers as downshifters and downconverters.

**Keywords:** CeO<sub>2</sub>, ceria, rare earths, photon-conversion, lanthanides, photovoltaics

## 1. Introduction

The peculiar chemical and magnetic properties of  $\text{CeO}_2$  related to its partially filled 4f shell, together with the excellent mechanical properties and thermal stability, have favored the use of this material in a wide range of applications, such as in polishing,<sup>1</sup> in catalysis,<sup>2-5</sup> in Li-ion batteries<sup>6</sup> and in solid oxide fuel cells.<sup>7,8</sup>

From the chemical point of view,  $\text{CeO}_2$  is particularly interesting because of its natural non-stoichiometry related to the presence of oxygen vacancies, which makes  $\text{CeO}_2$  an excellent redox material. In this sense,  $\text{CeO}_2$  is usually described as a material with a mixed-valence, in which the Ce valence fluctuates between 3+ (in  $4f^1(v)$  configuration due to a vacancy (v) in the O 2p states) and 4+ (with  $4f^0$  configuration).<sup>9-15</sup> The 4f electron occupation value can be as high as 0.4-0.5 and is expected to reach the highest values in nanostructured  $\text{CeO}_2$  due to the increased surface-to-volume ratio. The mixed valence state characterizes also other rare earth oxides ( $\text{TbO}_2$ ,  $\text{PrO}_2$ ) and gives rise to a rich phase diagram. In the case of  $\text{CeO}_2$ , the existence of this mixed valence state has been evidenced by analyzing the 3d photoemission spectra.<sup>16</sup>

A successful theoretical approach for calculating the band structure of  $\text{CeO}_2$  uses the Heyd-Scuseria-Ernzerhof (HSE) hybrid functional theory.<sup>17</sup> The authors showed that in stoichiometric crystals of  $\text{CeO}_2$ , the electronic states close to the Fermi level are divided in three bands mainly composed of hybridized O 2p, Ce 4f and Ce 5d states. The Ce 6s states take also part in the mix, because they are quite spread in energy, but the density of states is low and they will therefore not be considered here. In  $\text{CeO}_2$ , the lowest electronic transitions occur between a relatively large band below the Fermi level, which is mainly composed of O 2p occupied states, and a narrow band formed by the Ce 4f empty states, which lays about

3.6 eV<sup>18-20</sup> higher in energy. CeO<sub>2</sub> is therefore transparent to visible light and has a refractive index between 2 and 2.4.<sup>21,22</sup> These values are similar to those of the large band gap semiconductors typically used in photovoltaics and optoelectronics (ITO, ZnO, GaN and SiN<sub>x</sub>).

The large absorption cross section in the near UV range associated to the high transparency to visible wavelengths create a potential for this material in photon-conversion processes.

In particular, a UV photon can be converted into one or two visible or near-infrared photons using down-shifting and down-conversion processes, respectively.<sup>23</sup>

Other properties of CeO<sub>2</sub> contribute in making it a promising material for photon management. Among them, the most important are the small optical phonon energy (465 cm<sup>-1</sup> ≈ 58 meV<sup>24,25</sup>) compared to other oxides and the large ionic radius of Ce<sup>4+</sup> (~90 pm),<sup>26</sup> which favors the insertion of dopants.

CeO<sub>2</sub> organizes in a cubic fluorite-type lattice where the Ce sites have cubic O<sub>h</sub> symmetry and where the Ce<sup>4+</sup> ions are coordinated to 8 oxygen atoms.<sup>27</sup> The lattice constant of 5.411 Å make this material particularly promising for application in silicon-based devices.<sup>28</sup>

Although Ce is a rare earth and therefore one of the elements possessing the discrete electronic levels necessary to photon management, the low electron occupation value (lower than 1) of the 4f shell strongly reduces the number of 4f energy levels on a Ce ion (up to 2 multiplets in the case of a Ce<sup>3+</sup> ion), and therefore limits the available optical transitions. An interesting way to boost the photon management properties is to dope this material with other rare-earth ions having a richer diagram. Particularly interesting for down-shifting and down-conversion would be the situation in which one could combine the high UV absorption of CeO<sub>2</sub> with the emission properties of the dopants. This is possible only if the energy absorbed by CeO<sub>2</sub> efficiently transfers to the lanthanide dopants.

With respect to other RE-doped oxides (glasses or ceramic materials), RE doping into CeO<sub>2</sub>

has been relatively less studied in regards of photon conversion. In the last decade, however, the interest for this material has grown considerably. An extensive investigation of lanthanide doped ceria and ceria/zirconia material has been carried out by the group of Tiseanu.<sup>29-34</sup> Their work particularly focuses on the role of the symmetry of the lattice site and of the ionic radius on the emission properties of these materials. The up-conversion (a process in which several photons are combined to produce a single higher-energy photon) properties in three-dimensionally ordered macroporous  $\text{CeO}_2$ :  $\text{Er}^{3+}$ ,  $\text{Yb}^{3+}$  have been investigated by Wu *et al.*<sup>35</sup> and very recently by Carvalho *et al.* in precipitated  $(\text{Tm}^{3+}/\text{Yb}^{3+}/\text{Ho}^{3+})$ : $\text{CeO}_2$ .<sup>36</sup> The structural and luminescent properties of  $\text{CeO}_2$ : $\text{Eu}^{3+}$  and  $\text{CeO}_2$ : $\text{Sm}^{3+}$  thin films have been investigated by Fujihara and Oikawa,<sup>37</sup> Li *et al.*<sup>38</sup> and Wu *et al.*<sup>39</sup> Additional work has been done by Kunimi and Fujihara,<sup>40</sup> who successfully obtained red pigments using  $\text{CeO}_2$  doped with  $\text{Pr}^{4+}$  and  $\text{Eu}^{3+}$ . In addition, Wang *et al.*<sup>41</sup> showed how self-doping of  $\text{CeO}_2$  with  $\text{Ce}^{3+}$  can enhance the energy transfer to  $\text{Tb}^{3+}$ , while Kumar *et al.*<sup>42</sup> that the concentration of  $\text{Ce}^{3+}$  and oxygen vacancies strongly affects the emission.

On our side, we also believe that self-doping with  $\text{Ce}^{3+}$  ions is crucial to the luminescence properties of lanthanides in  $\text{CeO}_2$ . While most research groups suggest that the lanthanide emission occurs through a charge transfer mechanism between the O 2p band and the Ce 4f band of  $\text{CeO}_2$ ,<sup>33,43</sup> in this work we give experimental evidence indicating that the energy transfer occurs through intrinsic  $\text{Ce}^{3+}$  ions in  $\text{CeO}_2$ . In addition, while most of the works cited above are carried out using powders, we try to evaluate the potential of RE-doped (RE = Nd, Yb, Sm)  $\text{CeO}_2$  films for potential applications in the field of photovoltaics. The films have been grown using pulsed laser deposition. The structural and optical properties are compared between the different rare earths in an effort to understand the transfer mechanisms. The information obtained by comparing the absorbance and

photoluminescence data with the structural analyses enables us to infer the optical activation of the dopants and to gain insight in the energy transfer mechanisms with the host.

## 2. Experimental

The (RE):CeO<sub>2</sub> thin films were grown on silicon (100) substrates using pulsed laser deposition (PLD) starting from in-house sintered targets. The preparation of RE-doped CeO<sub>2</sub> targets was carried out by solid state reaction of the oxides from the stoichiometric mixture of the elemental oxide powders. The details on the preparation process can be found in our previous work.<sup>44</sup>

A KrF excimer laser (248 nm) was used for ablation. The deposition parameters yielding the best PL properties have been identified as a laser power of 25 mJ, a frequency of 10 Hz and an oxygen partial pressure of 0.001 mbar. The film thickness was around 100 nm. Despite the fact that the best emission results are obtained at temperatures above 500 °C, a substrate temperature of 400 °C during growth has been selected as the optimal temperature for possible application on inorganic solar cells.

The choice of the PLD technique has been driven by the fact that the targets are easy to prepare and that this technique is known to allow a complex stoichiometry transfer from the target to the film.<sup>45</sup> However, we expect that our results can be easily reproduced using sputtering, a technique which is more suitable to current large-scale solar cell technology.

The choice to work with Nd and Yb has been driven by the potential PL emission around 1000 nm, which is compatible with the band gap of silicon and therefore with most electronic and solar cell devices. As for Sm, this rare earth has great potential both in optoelectronic devices and in silicon solar cells, if involved in a cooperative process with a

second rare earth.

Several concentrations of the different rare earths have been tested, ranging from 1 to 10 %. The indicated concentrations are the nominal ones. Indeed, the measurement of the concentration of elements that are so close in the periodic table (Ce is a rare earth itself), quite low in concentration (a few percent) and in such a small quantity (100 nm of film) is quite difficult by most of the common techniques, such as Rutherford backscattering (RBS) and energy-dispersive x-ray (EDX) spectroscopies. EDX analysis performed on the doped PLD targets before deposition is reported in the supplementary material (Figure S1). The measurements have been performed using a JEOL JSM-6700F scanning electron microscope (SEM) at an operating voltage of 15 kV and at a magnification of 500x. The acquisition time was typically between 1 to 3 minutes. No impurities could be evidenced by EDX on the pure target. We expect that, by using PLD, the impurity concentration of the films is close to that reported for the targets.

The crystalline structure of the films was analyzed using a Rigaku SmartLab® X-ray diffractometer equipped with a Ge(220)x2 monochromatic source delivering a Cu K $\alpha$ 1 radiation (45 kV, 200 mA,  $\lambda=0.154056$  nm). The crystallite size and the lattice parameter along the growth direction have been calculated using Scherrer's formula and Bragg's law. The density of the films has been obtained by x-ray reflectivity (XRR) measurements.

Further insight on the structural properties and morphology of the samples was obtained by cross-section transmission electron microscopy (TEM) using a JEOL 2100 F microscope Cs corrected at the probe level, with a point to point resolution of 2 Å. The samples were prepared by mechanical polishing followed by ion beam milling using a Gatan Precision Ion Polishing System.

The film thickness and absorption coefficient were obtained using a HORIBA Uvisel™ Lt M200 FGMS (210–880 nm) spectroscopic ellipsometer. The used fitting model was the Adachi new-Forouhi model included in the DeltaPsi2® software by HORIBA.

Photoluminescence (PL) measurements were carried out in order to unravel details on the insertion and activation of RE dopants in CeO<sub>2</sub>. With this technique, the electronic level structure of RE<sup>3+</sup> ions and the energy transfer from the host matrix (CeO<sub>2</sub>) to the RE ions can be analyzed as well. The excitation was provided by both the (10 mW) 325 nm line of a He-Cd laser and a broad-spectrum Energetiq® EQ-99FC laser-driven light source (LDLS™) equipped with a monochromator (the output power was of the order of 10 μW). The PL signals were recorded using an N<sub>2</sub>-cooled CCD camera. Low-temperature PL was measured at about 15 K. For this purpose, the samples were mounted on a cold finger inside a vacuum-loading (He)-continuous-flow cryostat (Oxford MicrostatHe). Precise temperature control was obtained using an ITC temperature controller.

For the time-resolved PL, sub-picosecond excitation pulses at 343 nm were generated using a Tangerine (Amplitude Systems) amplified fiber laser system operating between 1 and 100 kHz. The time-resolved spectra were recorded using a Hamamatsu Streak Camera in photon counting mode, coupled to a spectrograph.

Particular attention was paid to eliminate parasitic luminescence originating from the environment and from the excitation by using a set of filters. The spectra presented here have been corrected for the filter and lamp emission, as well as for the detector response.

Element-specific near edge X-ray absorption fine structure (NEXAFS) spectroscopy was used to investigate the Ce valence in CeO<sub>2</sub> films. Spectroscopic measurements at Ce L<sub>2,3</sub> edge were performed at the Resonant Elastic-Inelastic X-ray Scattering (REIXS) beamline of the Canadian Light Source (CLS). The Ce L<sub>2,3</sub> NEXAFS spectra were obtained in total electron yield

(TEY) mode at a 45° angle of incidence and were normalized to the incoming photon flux as recorded by Au mesh to a constant background at 980 eV.

### 3. Results and discussion

Figure 1 reports the X-ray diffraction patterns (XRD) of the undoped and RE-doped CeO<sub>2</sub> films grown at 400 °C. All diffraction peaks indicate the formation of the cubic CeO<sub>2</sub> structure. No spurious phases related to Ce or RE oxides are observed within the detection limits of the XRD technique.

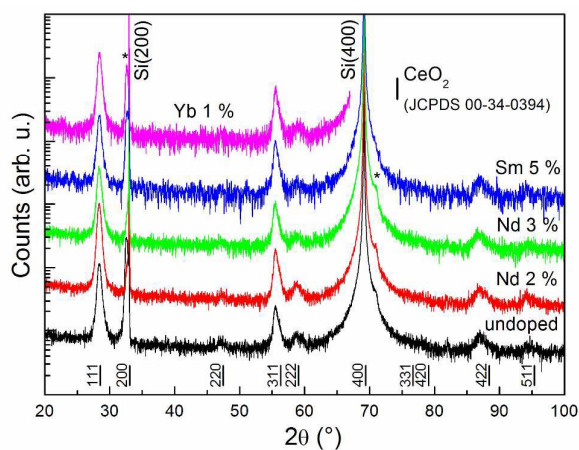


Figure 1 – XRD patterns of the CeO<sub>2</sub> films. The peak positions of cubic CeO<sub>2</sub> (JCPDS 00-034-0394) are reported for reference. The peaks marked with an asterisk in close proximity of the Si peaks are artifacts that are often observed in our setup when measuring Si (100) substrates.

The lattice parameter and the crystallites size calculated on the (111) peak have the same values for all films and are about  $a = 5.44 \pm 0.01 \text{ \AA}$  and  $D = 11 \pm 2 \text{ nm}$ , respectively. The lattice parameter is slightly higher for our films compared to the theoretical value (5.411 Å) and reflects the existence of a tensile stress, probably due to oxygen vacancies. The absence of variation in the crystallites size upon doping can be attributed to the sufficiently high deposition temperature (400 °C) that favors the formation of the cubic CeO<sub>2</sub> phase and to

the small mismatch of ionic radius between Ce and the other rare earths. The relative intensity of the diffraction peaks is not that observed for randomly oriented  $\text{CeO}_2$  powders (JCPDS card 34-394 of the ICDD database). In particular, the (220) peak (expected for  $\text{CeO}_2$  grown epitaxially on Si) is strongly suppressed and the film grows with few preferential directions (mainly [111] and [311]), that are those in which dense atomic planes are parallel to the surface of the substrate. This is due to the thin amorphous native oxide film that forms on the Si surface. The polycrystalline nature of the films and the absence of epitaxy are confirmed by TEM microscopy. A typical high-resolution cross section image of  $\text{CeO}_2$  films grown on Si at  $400^\circ\text{C}$  is shown in Fig. 2, while the selected area diffraction (SAED) pattern and the low resolution image are reported in Fig. S2. All the observations suggest that the films are dense, continuous and present a polycrystalline character.

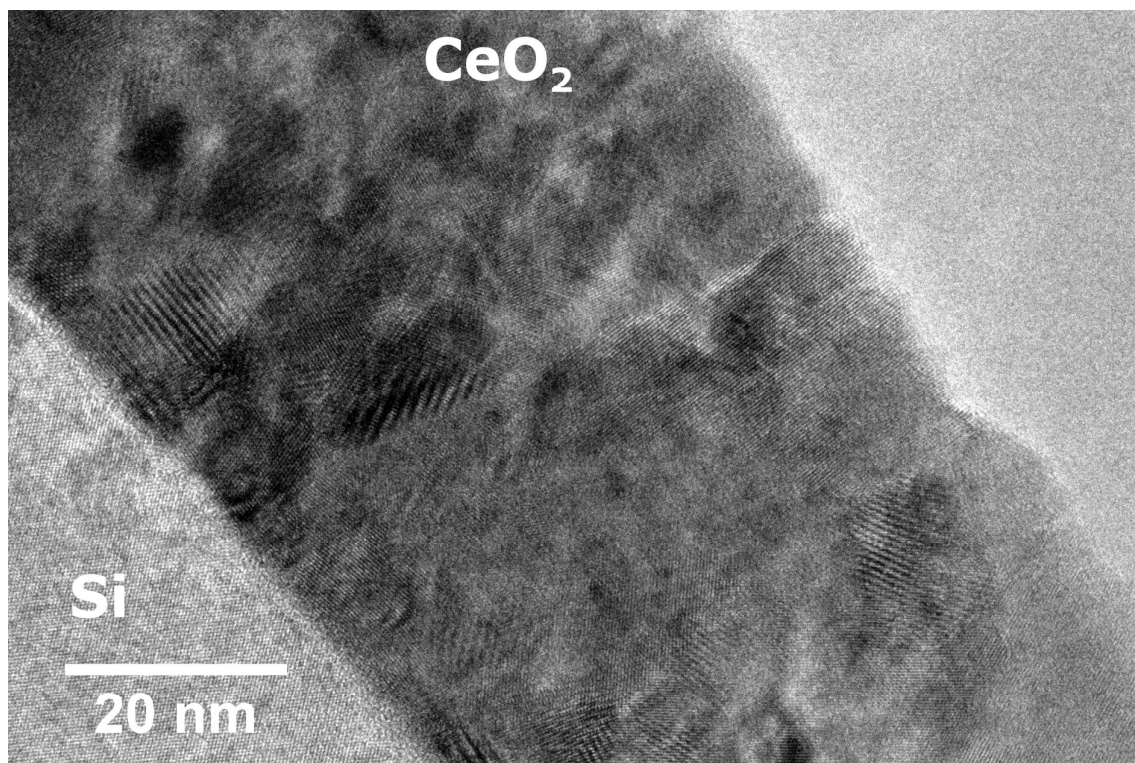


Figure 2 - HR-TEM cross section detail of a typical  $\text{CeO}_2(\text{:RE}^{3+})$  film grown on silicon at  $400^\circ\text{C}$ .

The high density of the films that can be observed in the TEM images is consistent with that estimated from XRR measurements,  $7.7 \pm 0.1 \text{ g/cm}^3$ , a value that is close to the theoretical density of  $7.65 \text{ g/cm}^3$ . This is compatible with the large value of the refractive index (2.5). As it can be observed in Figure S3 (see supplementary material), this value is particularly interesting for photovoltaics, as it matches very well the optimal refractive index of an anti-reflective coating between glass or ethyl vinyl acetate (EVA) and silicon.

More insight on the oxidation state of Ce is obtained by observing the NEXAFS measurements at X-ray absorption edge. Figure 3 shows as an example the Ce  $L_{2,3}$  NEXAFS spectrum of a Nd-doped  $\text{CeO}_2$  film compared to a high-purity  $\text{CeO}_2$  powder reference. It is clear that the Nd-doped film exhibits similar spectral features at both the  $L_3$  and  $L_2$  edges with the  $\text{CeO}_2$  powder reference representing  $\text{Ce}^{4+}$  valence except a small shoulder at 879 eV. This shoulder indicates the presence of  $\text{Ce}^{3+}$  in the Nd-doped film when compared to the Ce  $L_{2,3}$  XAS spectrum of  $\text{CeF}_3$  in ref. <sup>46</sup>

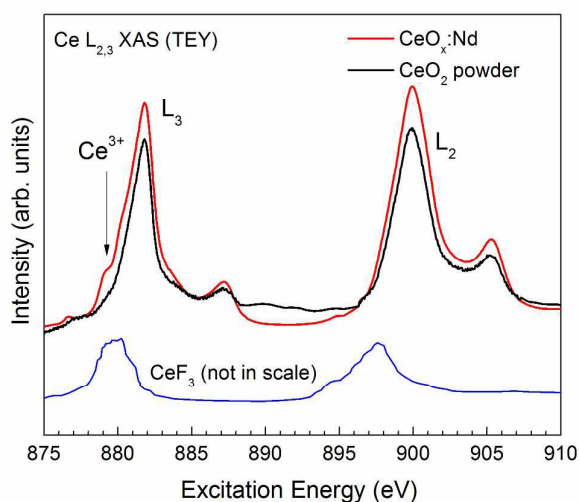


Figure 3 – Ce  $L_{2,3}$  XAS (TEY) measurement of Nd-doped  $\text{CeO}_2$  film obtained in total electron yield (TEY) mode. The spectrum of  $\text{Ce}^{4+}$  in a high-purity  $\text{CeO}_2$  powder reference and that of  $\text{Ce}^{3+}$  in  $\text{CeF}_3$  (Reproduced from R. Ishikawa et al., *Sci. Rep.*, 4 (2014) 3778. Licensed under a Creative Commons

Attribution 3.0 Unported License <http://creativecommons.org/licenses/by/3.0/> are reported for reference.

Unlike the case of  $\text{Ce}^{3+}$ , which has only one 4f excited state in the far infrared, the oxidation state of most rare earths can be guessed from the investigation of the optical properties thanks to the very specific emission/absorption pattern. To this purpose, the PL emission spectra have been recorded under 325 nm He-Cd laser excitation. The most representative data for the undoped and doped films are presented in Figure 4. The first observation that can be made is that the emission spectrum of the undoped  $\text{CeO}_2$  film is already very rich. The emission is characterized by several emission bands, each composed of a large number of narrow peaks. Given the number of peaks and the small peak widths, these peaks can neither be attributed to  $\text{Ce}^{3+}$  ions, whose unique 4f excited state is situated about 0.3 eV above the fundamental state, nor to defects in  $\text{CeO}_2$ . Curiously, such an emission spectrum is typical of other trivalent RE ions, which have a rich 4f energy level diagram. Since the impurities usually contained in commercial RE oxides are mainly RE impurities, this emission is not surprising. However, the fact that intense PL signals are recorded indicates that a large amount of dopant ions is optically active. In fact, given the high purity of the powder used to prepare the targets (99.95 %), the overall impurity concentration must be below 0.05 %.

Most of the observed peaks in the visible region of the spectrum can be attributed to  $\text{Sm}^{3+}$  impurities,<sup>38</sup> while the near infrared peaks can be attributed to  $\text{Nd}^{3+}$ .<sup>47</sup> As the EDX technique is not sensitive enough to detect such low impurity concentration, an ICP-MS measurement was carried out on the undoped target. The results indicate that indeed Sm is the main impurity with a concentration of about 0.013 at%. Traces of Yb, La and Ca were also evidenced with a concentration below 0.003 at%. No traces of Nd were detected, within the

limits of the ICP-MS technique. Finally, this measurement underlines the particular sensitivity of the PL technique to very low concentrations of (optically active) RE dopants.

If we now focus on the doped films, we can clearly observe that intentional doping with Sm and Nd strongly increases the specific emissions (note the logarithmic scale). Doping with Yb adds an emission band centered at 975 nm and composed of few narrow peaks, which can be associated to  $^2F_{5/2} \rightarrow ^2F_{7/2}$  transitions in  $\text{Yb}^{3+}$ .<sup>48, 49</sup>

Thus in Figure 4, all the observed emission bands could be roughly attributed to the specific 4f transitions. However, the identification of each individual peak is particularly complicated, due to the Stark splitting of the 4f multiplets (when a trivalent lanthanide substitutes for a  $\text{Ce}^{4+}$  ion, the symmetry of the lattice site is lowered<sup>33, 34</sup>), to the superposition of the emission lines of the different rare earths and, in general, to the very large number of peaks. The existence of several active sites is also very probable.

Compared to other oxide hosts, such as  $\text{ZnO}$ <sup>47, 48, 50</sup> and  $\text{SnO}_2$ <sup>51, 52</sup>, the peaks are narrower. This suggests that the active sites are characterized by a very small lattice disorder and that the phonon broadening is weak.

It is important to note that, given the absence of excited states of  $\text{Yb}^{3+}$  in the UV region of the spectrum, it can be asserted that some energy transfer must occur from the host to the  $\text{Yb}^{3+}$  sites. The possible resonance of the laser excitation with Sm and Nd transitions prevents us from drawing the same conclusion at this stage.

Figure 4 only reports the emission below 500 nm as no emission has been recorded between 350 and 550 nm. This range is where both the emission related to the Ce 4f - O 2p transition related to the  $\text{CeO}_2$  matrix and the f-d transitions related to  $\text{Ce}^{3+}$  ions are expected.<sup>17, 33, 44</sup> The fact that this emission is not observed even for the undoped film might be due to the rare-earth impurities found in the powder and might indicate that energy

transfer is particularly efficient. Unfortunately, we did not have a high purity undoped film for comparison.

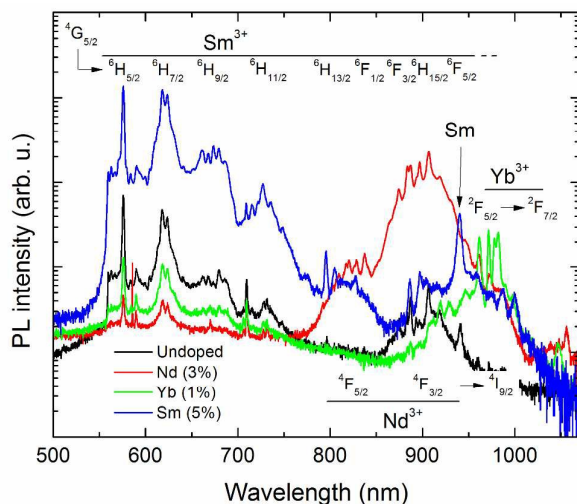


Figure 4 – Selected PL emission spectra of undoped and RE-doped CeO<sub>2</sub> films under 325 nm He-Cd laser excitation.

More insight into the transfer mechanisms can be obtained if the PL intensity of the RE<sup>3+</sup> emission is recorded as a function of the excitation wavelength. Figure 5 reports the PLE spectra of the 618 nm emission line of Sm<sup>3+</sup> and the 905 nm emission line of Nd<sup>3+</sup>. The PLE spectra are characterized by a relatively wide absorption feature centered at 350 nm just below the absorption edge of the host. This feature, which is common to all films, corresponds to indirect excitation of the host. Our previous work<sup>44</sup> on RE-doped pellets indicated that this absorption band is more likely ascribed to isolated Ce<sup>3+</sup> ions, rather than to Ce 4f – O 2p transitions as usually suggested in the literature.<sup>33, 37, 43</sup> This is in agreement with the fact that the formation of clusters of Ce<sup>3+</sup>, oxygen vacancies and trivalent rare earth ions is energetically favored in CeO<sub>2</sub>.<sup>53</sup> This spontaneous cluster formation is more effective when the films are grown at high temperatures ( $\geq 400$  °C), as for these temperatures the

ionic conductivity strongly increases. With respect to pure  $\text{CeO}_2$ , in RE doped ceria the ionic conductivity is even higher at a given temperature.<sup>54,55</sup> The existence of  $\text{Ce}^{3+}$  ions confirmed by the Ce  $L_{2,3}$  NEXAFS data supports this hypothesis. The fact that the  $\text{RE}^{3+}$  ions can be excited through  $\text{Ce}^{3+}$  ions indicates that the insertion of  $\text{RE}^{3+}$  in  $\text{CeO}_2$  is often accompanied by that of  $\text{Ce}^{3+}$  in close proximity, and that efficient transfer occurs between the two  $3+$  ion species. The presence of dimers and triplets of rare-earth-ions in charge-compensated materials is not unusual<sup>56</sup> and the high mobility of the oxygen vacancies in  $\text{CeO}_2$  (which can virtually “move” the  $\text{Ce}^{3+}$  ions)<sup>57,58</sup> might particularly favor these situations. It is clear that at small excitation power, the direct excitation of trivalent ions, which is barely visible, is less efficient than indirect excitation.

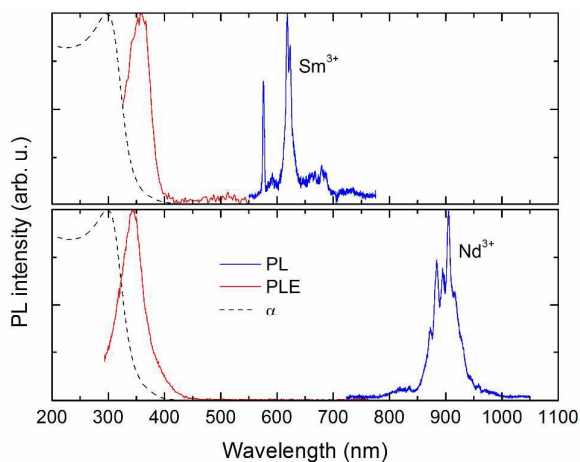


Figure 5 - PLE spectra of the 618 and 905 nm emission lines of  $\text{Sm}^{3+}$  and  $\text{Nd}^{3+}$ , respectively. The absorption coefficient calculated from ellipsometric data is added for reference.

More insight into the complex luminescence spectra can be obtained by measuring the emission at temperatures approaching that of liquid He. At such low temperatures, the phonon-related emission peaks are strongly suppressed and the observed peaks should be

related only to the Stark multiplicity of the levels generating the transition. As it can be observed in Fig. 6 for Sm and Nd, the low temperature has also the effect of reducing the population of the higher levels of the starting multiplet, which are thermally populated. Therefore, at low temperature the high-energy part of each band is suppressed. We also observe that the number of lines observed at 15 K largely exceeds the maximum multiplicity  $(2J+1)/2$  of each term, thus proving the existence of at least two optically active sites for the trivalent RE ions.

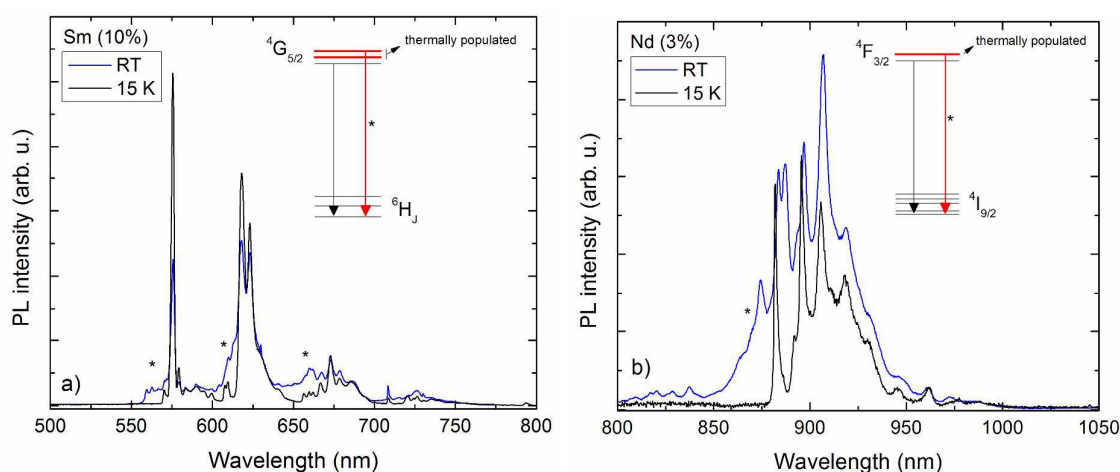


Figure 6 - RT and low temperature PL spectra of a)  $\text{Sm}^{3+}$  and b)  $\text{Nd}^{3+}$  in  $\text{CeO}_2$ .

Figure 7 reports the time-resolved PL signals emitted by Sm- and Nd-doped  $\text{CeO}_2$  films under 343 nm pulsed laser excitation. By combining the results obtained at different time scales ranging from 100 ns to 1 ms, we observe that the decay profiles can be conveniently fitted by a multiple exponential. The intensity of the collected signal was too weak to measure over longer time frames. In particular, the emission coming from Nd ions is weaker than that of Sm and is situated closer to the detection limit of our Si detector. Therefore, the decay profile of this rare earth could not be observed in the millisecond range. For the same

reason, and because the emission of Yb in our films is one order of magnitude weaker than the signal of Nd, the TR-PL signal of Yb could not be observed at all. The signal is typically composed of the following decay times: 10 ns, 100 ns, 2-3  $\mu$ s, 20  $\mu$ s and 150  $\mu$ s. This probably means that several emission lines are superimposed, which are associated to different relaxation processes. This is also suggested by the fact that the decay time of the transitions from the thermally populated states (high-energy side of the peaks) is slightly longer than that of the transition occurring from the fundamental state. However, the absence of an appropriate wavelength resolution prevents us from deconvoluting the different signals.

The relatively long lifetime of some transitions is typical of the dipole-forbidden 4f transitions on RE ions and many authors reported lifetimes in or above the millisecond scale.<sup>31, 33, 38, 41</sup> Decay constants at the scale of tenths and a hundred microseconds can be also expected from trivalent RE ions.<sup>49, 59</sup> Shorter decay times might be due to the competition with non-radiative recombination paths.

Since the lifetime of the excited state also depends on the symmetry of the lattice environment, the superposition of several signals with different time constants might be interpreted as a proof of the existence of several active sites for the RE<sup>3+</sup> ions in CeO<sub>2</sub>.

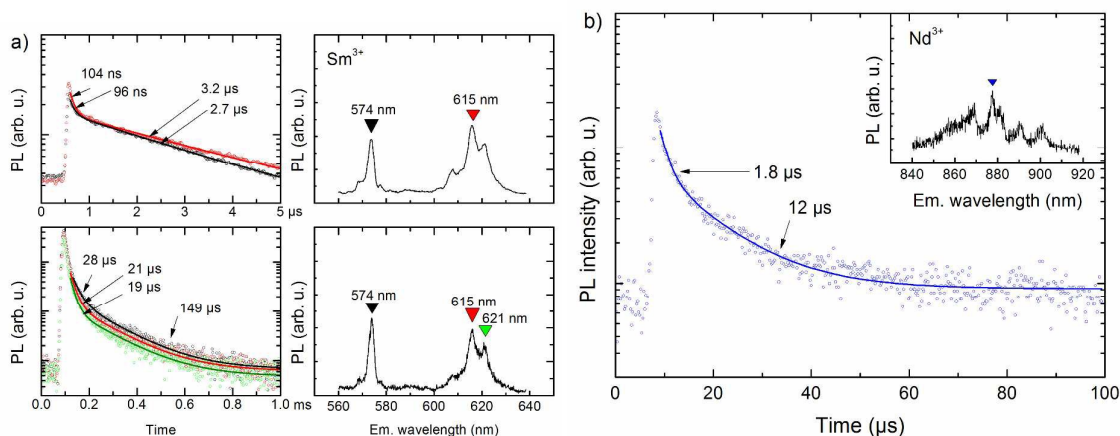


Figure 7 – PL spectra and TR-PL profiles of the main emission lines of a)  $\text{Sm}^{3+}$  and b)  $\text{Nd}^{3+}$  in  $\text{CeO}_2$  (observed at different timescales).

All these results create a coherent picture in which the trivalent RE ions are inserted in the films at least in two different lattice sites, and the energy transfer occurs from sensitizing  $\text{Ce}^{3+}$  ions that are intrinsic in our  $\text{CeO}_2$  films. As represented in Fig. 8, this energy transfer occurs through f-d transitions on  $\text{Ce}^{3+}$  ions. Since Sm and Nd have a rich energy level diagram, the transfer probably relies on the resonance between the 5d-4f transitions on  $\text{Ce}^{3+}$  and some 4f-4f transition on the trivalent dopants. The resonance with different 4f levels could explain the slightly different position of the indirect transfer band observed in Fig. 5.

Figure 8 also shows that Yb ions cannot be excited through the same transfer mechanism, as its unique 4f excited state multiplet is situated only 1.3 eV above the ground state. Yet, we observe Yb emission in the PL spectra. A possible mechanism could involve the transfer from a  $\text{Ce}^{3+}$  ion to two  $\text{Yb}^{3+}$  ions leading to a phonon-assisted down conversion of a 3 eV photon into two 1.3 eV photons, but the energy mismatch of 400 meV is quite large and this process would involve too many phonons to be realistic. However, if we consider relaxation through the  $5d-^2F_{7/2}$  transition on  $\text{Ce}^{3+}$ , the gap is reduced to about 100 meV, that is less than twice the energy of the optical phonon of  $\text{CeO}_2$  (58 meV). The decay time of this

process is expected to be different from that of Sm and Nd, but unfortunately the emission of Yb was too far in the infrared for our TR-PL setup. This  $\text{Ce}^{3+}$ - $\text{Yb}^{3+}$  down-conversion process has been theoretically investigated by Boccolini *et al.*<sup>60</sup> An alternative explanation for the energy transfer might involve the deep defect levels created by oxygen vacancies or other point defects in  $\text{CeO}_2$ .<sup>61</sup> However, no radiative transitions are observed due to defects, even in films presenting only a small quantity of rare-earth impurities (< 0.05 %).

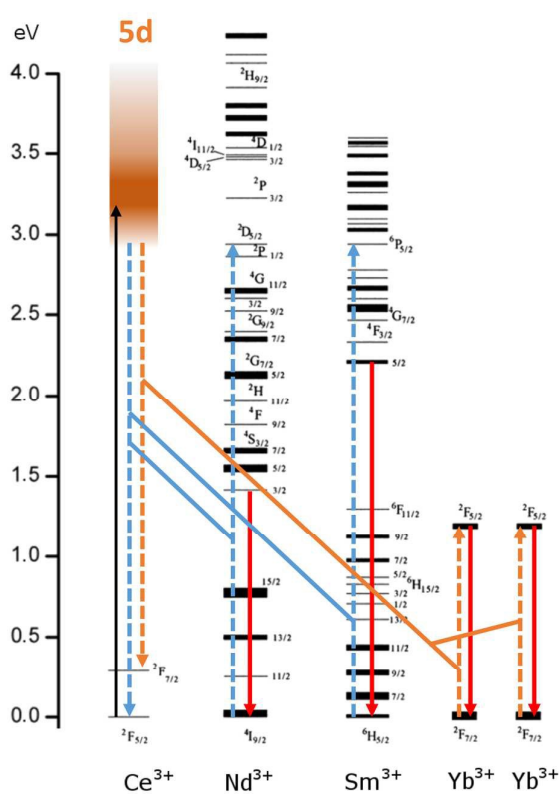


Figure 8 - Schematic of the energy transfer mechanisms based on intrinsic  $\text{Ce}^{3+}$  ions in RE-doped  $\text{CeO}_2$  films. The energy level diagram of the trivalent RE ions has been taken from ref.<sup>62</sup> and is relative to  $\text{LaCl}_3$  as a host. The dashed arrows and the oblique lines represent the transfer mechanisms. The plain arrows indicate some observed radiative transitions.

#### 4. Conclusion

$\text{CeO}_2$  films doped with trivalent Nd, Sm and Yb ions have been successfully prepared by

pulsed laser deposition. The structural analysis showed that the insertion of trivalent lanthanides does not alter significantly the CeO<sub>2</sub> lattice and the compositional analysis evidenced the presence of Ce<sup>3+</sup> ions in the films.

The ellipsometric data show that the optical constants of CeO<sub>2</sub> films are compatible with silicon optoelectronics.

The existence of RE ions in the trivalent form is proven by the observation of the typical emission patterns in the PL spectra. Despite the large number of emission lines, most transitions could be attributed to the respective term symbols.

The low temperature PL measurements showed that the number of emission lines in the PL spectra observed at 15 K exceeds the multiplicity of the levels, which suggests the existence of several active sites for the RE<sup>3+</sup> ions. In addition, the comparison with the room temperature PL indicates that the higher Stark levels of each multiplet are thermally populated. The transient PL suggested slightly longer lifetimes for these states and also supports the hypothesis of several active sites for the RE<sup>3+</sup> ions.

From the measurement of the PL excitation spectra, we found that energy transfer occurs from sensitizing Ce<sup>3+</sup> ions that are intrinsic in our CeO<sub>2</sub> films. The emission intensity associated to this indirect mechanism is much stronger than that coming from the direct excitation of the trivalent RE ions. A transfer mechanism has been proposed, based on the resonance between the f-d transitions of Ce<sup>3+</sup> and some f-f transitions on Sm and Nd. The transfer is different in the case of Yb, where two Yb ions are possibly involved in a phonon-assisted down-conversion process occurring through the 4f <sup>2</sup>F<sub>7/2</sub> excited state of Ce<sup>3+</sup>.

#### ACKNOWLEDGEMENTS

The authors thank the Rhin Solar INTERREG project n° C25 and the French Ministry of

Education and Research for financial support.

Research described in this paper was performed at the Canadian Light Source (CLS), which is supported by the Canadian Foundation for Innovation, Natural Sciences and Engineering Research Council of Canada (NSERC), the University of Saskatchewan, the Government of Saskatchewan, Western Economic Diversification Canada, the National Research Council Canada, and the Canadian Institutes of Health Research. Spectroscopic measurements at CLS were supported by NSERC Discovery Grant.

The authors thank Corinne Ulhaq-Bouillet for her contribution to the TEM observation, Cédric Leuvrey for performing the EDX analysis and Anne Boos for the ICP-MS analysis.

## References

1. N. B. Kirk and J. V. Wood, *British Ceramic Trans.*, 1994, **93**, 25–30.
2. N. J. Lawrence, J. R. Brewer, L. Wang, T.-S. Wu, J. Wells-Kingsbury, M. M. Ihrig, G. Wang, Y.-L. Soo, W.-N. Mei and C. L. Cheung, *Nano Letters*, 2011, **11**, 2666-2671.
3. B. Murugan and A. V. Ramaswamy, *J. Am. Chem. Soc.*, 2007, **129**, 3062-3063.
4. A. D. Mayernick and M. J. Janik, *J. Phys. Chem. C*, 2008, **112**, 14955-14964.
5. B. R. Powell, R. L. Bloink and C. C. Eickel, *J. Am. Ceram. Soc.*, 1988, **71**, C-104-C-106.
6. H. Pang and C. Y. Chen, *RSC Adv.*, 2014, **4**, 14872-14878.
7. J. Van Herle, T. Horita, T. Kawada, N. Sakai, H. Yokokawa and M. Dokiya, *J. Am. Ceram. Soc.*, 1997, **80**, 933-940.
8. W. Liu, B. Li, H. Liu and W. Pan, *Electrochim. Acta*, 2011, **56**, 8329-8333.
9. T. K. Sham, R. A. Gordon and S. M. Heald, *Phys. Rev. B*, 2005, **72**, 035113 - 035113-035116.
10. G. Krill, J. P. Kappler, A. Meyer, L. Abadli and M. F. Ravet, *J. Phys. F Met. Phys.*, 1981, **11**, 1713-1725.
11. A. Bianconi, A. Marcelli, H. Dexpert, R. Karnatak, A. Kotani, T. Jo and J. Petiau, *Phys. Rev. B*, 1987, **35**, 806-812.
12. H. Dexpert, R. C. Karnatak, J. M. Esteva, J. P. Connerade, M. Gasgnier, P. E. Caro and L. Albert, *Phys. Rev. B*, 1987, **36**, 1750-1753.
13. T. Jo and A. Kotani, *Solid State Commun.*, 1985, **54**, 451-456.
14. A. Kotani, T. Jo and J. C. Parlebas, *Adv. Phys.*, 1988, **37**, 37-85.
15. M. Nakazawa, S. Tanaka, T. Uozumi and A. Kotani, *J. Electron Spectrosc.*, 1996, **79**, 183-186.
16. T. Nakano, A. Kotani and J. C. Parlebas, *J. Phys. Soc. Jpn.*, 1987, **56**, 2201-2210.
17. P. J. Hay, R. L. Martin, J. Uddin and G. E. Scuseria, *J. Chem. Phys.*, 2006, **125**, 034712-034711 - 034718.
18. S. Colis, A. Bouaine, G. Schmerber, C. Ulhaq-Bouillet, A. Dinia, S. Choua and P. Turek, *Phys. Chem. Chem. Phys.*, 2012, **14**, 7256-7263.

19. S. Guo, H. Arwin, S. N. Jacobsen, K. Järrendahl and U. Helmersson, *J. Appl. Phys.*, 1995, **77**, 5369-5376.
20. S. Colis, A. Bouaine, R. Moubah, G. Schmerber, C. Ulhaq-Bouillet, A. Dinia, L. Dahéron, J. Petersen and C. Becker, *J. Appl. Phys.*, 2010, **108**, 053910 - 053910-053916.
21. R. M. Bueno, J. M. Martinez-Duart, M. Hernandez-Velez and L. Vazquez, *J. Mater. Sci.*, 1997, **32**, 1861-1865.
22. K. Narasimha Rao, L. Shivlingappa and S. Mohan, *Mater. Sci. Eng. B-Solid*, 2003, **98**, 38-44.
23. B. S. Richards, *Sol. Energy Mater. Sol. Cells*, 2006, **90**, 2329-2337.
24. S. Wang, W. Wang, J. Zuo and Y. Qian, *Mater. Chem. Phys.*, 2001, **68**, 246-248.
25. I. Kosacki, T. Suzuki, H. U. Anderson and P. Colomban, *Solid State Ionics*, 2002, **149**, 99-105.
26. R. Shannon, *Acta Crystallogr. A*, 1976, **32**, 751-767.
27. K. Nakamoto, *Infrared and Raman Spectra of Inorganic and Coordination Compounds*, John Wiley & Sons, New York, 5<sup>th</sup> edn., 1997.
28. T. Inoue, Y. Yamamoto, S. Koyama, S. Suzuki and Y. Ueda, *Appl. Phys. Lett.*, 1990, **56**, 1332-1333.
29. D. Avram, C. Gheorghe, C. Rotaru, B. Cojocar, M. Florea, V. Parvulescu and C. Tiseanu, *J. Alloy Compd.*, 2014, **616**, 535-541.
30. D. Avram, M. Sanchez-Dominguez, B. Cojocar, M. Florea, V. Parvulescu and C. Tiseanu, *J. Phys. Chem. C*, 2015, **119**, 16303-16313.
31. A. Lupei, C. Tiseanu, C. Gheorghe and F. Voicu, *Appl. Phys. B*, 2012, **108**, 909-918.
32. V. I. Parvulescu and C. Tiseanu, *Catalysis Today*, 2015, **253**, 33-39.
33. C. Tiseanu, B. Cojocar, D. Avram, V. I. Parvulescu, A. V. Vela-Gonzalez and M. Sanchez-Dominguez, *J. Phys. D Appl. Phys.*, 2013, **46**, 275302 - 275302-275308.
34. C. Tiseanu, V. I. Parvulescu, M. Boutonnet, B. Cojocar, P. A. Primus, C. M. Teodorescu, C. Solans and M. S. Dominguez, *Phys. Chem. Chem. Phys.*, 2011, **13**, 17135-17145.
35. H. Wu, Z. Yang, J. Liao, S. Lai, J. Qiu, Z. Song, Y. Yang, D. Zhou and Z. Yin, *J. Alloy Compd.*, 2014, **586**, 485-487.
36. L. G. A. Carvalho, L. A. Rocha, J. M. M. Buarque, R. R. Gonçalves, C. S. Nascimento Jr, M. A. Schiavon, S. J. L. Ribeiro and J. L. Ferrari, *J. Lumin.*, 2015, **159**, 223-228.
37. S. Fujihara and M. Oikawa, *J. Appl. Phys.*, 2004, **95**, 8002-8006.
38. L. Li, S. W. Wang, G. Y. Mu, X. Yin, Y. Tang, W. B. Duan and L. X. Yi, *Phys. Status Solidi B*, 2013, **251**, 737-740.
39. J. Wu, S. Shi, X. Wang, J. Li, R. Zong and W. Chen, *J. Mater. Chem. C*, 2014, **2**, 2786-2792.
40. S. Kunimi and S. Fujihara, *ECS J. Solid State Sci. Technol.*, 2012, **1**, R32-R36.
41. X. Wang, D. Zhang, Y. Li, D. Tang, Y. Xiao, Y. Liu and Q. Huo, *RSC Adv.*, 2013, **3**, 3623-3630.
42. A. Kumar, S. Babu, A. S. Karakoti, A. Schulte and S. Seal, *Langmuir*, 2009, **25**, 10998-11007.
43. L. Li, H. K. Yang, B. K. Moon, Z. Fu, C. Guo, J. H. Jeong, S. S. Yi, K. Jang and H. S. Lee, *J. Phys. Chem. C*, 2009, **113**, 610-617.
44. M. Balestrieri, S. Colis, M. Gallart, G. Schmerber, M. Ziegler, P. Gilliot and A. Dinia, *J. Mater. Chem. C*, 2015, **3**, 7014 - 7021.
45. D. Dijkamp, T. Venkatesan, X. D. Wu, S. A. Shaheen, N. Jisrawi, Y. H. Min-Lee, W. L. McLean and M. Croft, *Appl. Phys. Lett.*, 1987, **51**, 619-621.
46. R. Ishikawa, A. R. Lupini, F. Oba, S. D. Findlay, N. Shibata, T. Taniguchi, K. Watanabe, H. Hayashi, T. Sakai, I. Tanaka, Y. Ikuhara and S. J. Pennycook, *Sci. Rep.*, 2014, **4**, 3778.
47. M. Balestrieri, S. Colis, M. Gallart, G. Ferblantier, D. Muller, P. Gilliot, P. Bazylewski, G. S. Chang, A. Slaoui and A. Dinia, *J. Mater. Chem. C*, 2014, **2**, 9182-9188.
48. M. Balestrieri, G. Ferblantier, S. Colis, G. Schmerber, C. Ulhaq-Bouillet, D. Muller, A. Slaoui and A. Dinia, *Sol. Energy Mater. Sol. Cells*, 2013, **117**, 363-371.
49. I. Soumahoro, G. Schmerber, A. Douayar, S. Colis, M. Abd-Lefdil, N. Hassanain, A. Berrada, D. Muller, A. Slaoui, H. Rinnert and A. Dinia, *J. Appl. Phys.*, 2011, **109**, 033708 - 033708-033705.
50. M. Balestrieri, M. Gallart, M. Ziegler, P. Bazylewski, G. Ferblantier, G. Schmerber, G. S. Chang, P. Gilliot, D. Muller, A. Slaoui, S. Colis and A. Dinia, *J. Phys. Chem. C*, 2014, **118**, 13775-13780.

51. H. Rinnert, P. Miska, M. Vergnat, G. Schmerber, S. Colis, A. Dinia, D. Muller, G. Ferblantier and A. Slaoui, *Appl. Phys. Lett.*, 2012, **100**, 101908 - 101908-101903.
52. K. Bouras, J. L. Rehspringer, G. Schmerber, H. Rinnert, S. Colis, G. Ferblantier, M. Balestrieri, D. Ihiwakrim, A. Dinia and A. Slaoui, *J. Mater. Chem. C*, 2014, **2**, 8235-8243.
53. D. R. Ou, F. Ye and T. Mori, *Phys. Chem. Chem. Phys.*, 2011, **13**, 9554-9560.
54. G. B. Balazs and R. S. Glass, *Solid State Ionics*, 1995, **76**, 155-162.
55. H. Inaba and H. Tagawa, *Solid State Ionics*, 1996, **83**, 1-16.
56. M. B. Seelbinder and J. C. Wright, *J. Chem. Phys.*, 1981, **75**, 5070-5079.
57. H.-F. Wang, H.-Y. Li, X.-Q. Gong, Y.-L. Guo, G.-Z. Lu and P. Hu, *Phys. Chem. Chem. Phys.*, 2012, **14**, 16521-16535.
58. A. Trovarelli, *Comment. Inorg. Chem.*, 1999, **20**, 263-284.
59. S. Q. Man, H. L. Zhang, Y. L. Liu, J. X. Meng, E. Y. B. Pun and P. S. Chung, *Opt. Mater.*, 2007, **30**, 334-337.
60. A. Boccolini, J. Marques-Hueso, D. Chen, Y. Wang and B. S. Richards, *Sol. Energy Mater. Sol. Cells*, 2014, **122**, 8-14.
61. S. Aškračić, Z. D. Dohčević-Mitrović, V. D. Araújo, G. Ionita, J. M. M. de Lima and A. Cantarero, *J. Phys. D Appl. Phys.*, 2013, **46**, 495306 - 495306-495309.
62. G. H. Dieke, *Spectra and Energy Levels of Rare Earth Ions in Crystals*, Interscience Publishers, New York, 1968.

TOC graphic

